Pattern Recognition Letters 149 (2021) 83–90

Contents lists available at ScienceDirect

Pattern Recognition Letters

journal homepage: www.elsevier.com/locate/patrec

Regularizer based on Euler characteristic for retinal blood vessel segmentation☆

Lukman Hakim[a], Muthu Subash Kavitha[b], Novanto Yudistira[c], Takio Kurita[d,*]

[a] Department of Information Engineering, Graduate School of Engineering, Hiroshima University, 1-4-1 Kagamiyama, Higashi-Hiroshima-shi, Hiroshima739-8527, Japan
[b] School of Information and Data sciences, Nagasaki University, 1-14 Bunkyo-machi, Nagasaki, Japan.
[c] Intelligent System Lab, Faculty of Computer Science, Brawijaya University, 8 Veteran Road Malang, Indonesia 65145, Indonesia
[d] Graduate School of Advanced Science and Engineering, Hiroshima University, 1-4-1 Kagamiyama, Higashi-Hiroshima-shi, Hiroshima739-8527, Japan

ARTICLE INFO

Article history:
Received 5 June 2020
Revised 25 March 2021
Accepted 18 May 2021
Available online 15 June 2021

MSC:
41A05
41A10
65D05
65D17

Keywords:
Fundus image
Segmentation
Euler characteristic
Regularizer

ABSTRACT

Segmentation of retinal blood vessels is important for the analysis of diabetic retinopathy (DR). Existing methods do not prioritize the small and disconnected vessels for DR. With the aim of paying attention to the small and disconnected vessel regions, this study introduced Euler characteristics (EC) from topology to calculate the number of isolated objects on segmented vessel regions, which is the key contribution of this study. In addition, we utilized the number of isolated objects in a U-Net-like deep convolutional neural network (CNN) architecture as a regularizer to train the network for improving the connectivity between the pixels of the vessel regions. The proposed network performance of the regularizer based on EC in reconstructing vessel regions is compared over the network without our regularizer. Furthermore, the capacity of the proposed regularizer approach in enhancing the smoothness and pixel connectivity of the vessels is compared with graph-based smoothing (GS) and combined GS with isolated objects (GISO) regularizers for delineating blood vessel regions. The proposed approach achieved the area under the curve value of 0.982, which is much higher than the state-of-the-arts, and thus it is suggested that the proposed system could support accuracy and reliability in decision-making for DR detection.

1. Introduction

Diabetic retinopathy (DR) is one of the causes of visual impairment in aging population and signifies an increased risk of coronary heart disease [1]. As it involves changes in the shape and structure of blood vessels in the fundus, visual impairment is often detected by analyzing fundus images. Fundus images are color images that represent the inner surface of the human eye and are often used by doctors to study at the retina and the anatomical components of the eye. Therefore, accurate identification of large and small retinal vessels with diameters of less than a pixel can be used as an early bio-marker for the diagnosis of DR [2,3].

However, fundus images are affected by noise. Moreover, examining the small blood vessels is difficult and time-consuming. Hence, automatic characterizing of retinal blood vessels is important for the detection of DR. To this end, computer-aided segmentation of retinal blood vessels, based on pattern recognition, and supervised and unsupervised machine learning, has been successfully proposed [4–6]. Various studies in recent times have reported improve performance of blood vessel segmentation based on deep learning techniques [7–13]. Several U-Net models based on convolutional neural networks (CNNs) have been developed by modifying the number of layers in the encoder and decoder architectures and have achieved better results for retinal blood vessel segmentation [9,14–16]. However, these approaches considered large and medium vessels as it appears in the ground truth. They failed to characterize the damaged tiny or small vessels, and hence unreliable diagnosis may occur. In this study, we aimed to delineate, in addition to the thick vessels, damaged tiny or small vessels that do not appear in the ground truth but appear in the original fundus images.

To address the small vessel connectivity problem, authors in [17] introduced a graph-based smoothing (GS) regularizer that pushes the network to consider small vessel. The GS regularizer hold smoothness level by calculating graph laplacians between the vessel and surrounding background area. In contrast, in this study, we proposed a different approach to penalize the network to pay more attention to small vessels by utilizing the number of isolated

☆ Handle by Associate Editor Michele Nappi, Ph.D.

* Corresponding author.
E-mail addresses: lukman-hakim@hiroshima-u.ac.jp (L. Hakim), kavitha@nagasaki-u.ac.jp (M.S. Kavitha), cbasemaster@gmail.com (N. Yudistira), tkurita@hiroshima-u.ac.jp (T. Kurita).

https://doi.org/10.1016/j.patrec.2021.05.023
0167-8655/

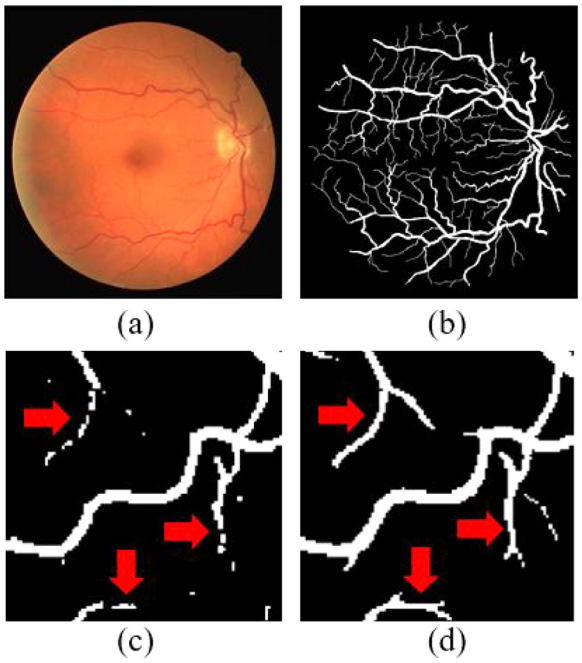

Fig. 1. Illustration of the isolated object in vessel segmentation task. (a) input fundus image. (b) groundtruth segmentation of the vessels. (c) result of the baseline without regularizer. (d) proposed isolated object regularizer (red color arrow indicates retaining the width of the small and disjointed vessel connectivities). (For interpretation of the references to color in this figure legend, the reader is referred to the web version of this article.)

objects, as shown in the Fig. 1. Furthermore, we observe that most of the existing architectures fail to accurately detect the vessel connections especially on the thinner and small branches of the vessels (Fig. 1c).

However, for accurate segmentation, it important to preserve the vanished blood vessels as isolated objects so as to use them for finding entire vessel connections. Hence, this study is attempted to trace the retinal vessel connections using Euler characteristics (EC). The EC is an essential topological invariant for realizing the number of components and number of enclosed cavities to utilize the EC as a demonstration of vessel connectivity [18,19].

We introduced a regularizer based on EC to minimize the number of isolated objects, especially in the small branches and tiny retinal vessel regions. The proposed method is based on the criterion of a vessel structure that is fully connected or if consisting of minimal number of isolated objects.

Specifically, we proposed two regularizers, minimum number of isolated objects (MISO) and differences of number of isolated objects (DISO) between predicted and true segmentation groundtruth based on EC, to delineate tiny vessel regions. We developed a U-Net-like CNN architecture to evaluate the performance of the proposed regularizers in delineating small vessel connections. The interesting key point in this study is implementing mathematical topology approach in the neural network architecture. The main contribution of this study is summarized as follows : (i) We proposed EC-based regularizers to estimate the number of isolated objects, (ii) compared the architecture performance of the proposed MISO and DISO regularizers with the architecture without regularizer, (iii) compared the performance of our proposed regularizers with GS and combined GS plus isolated objects (GISO) regularizers in segmenting the vessel connections, and (iv) analyzed the performance of the proposed approach with the state-of-the-art method for recognizing small blood vessel regions.

2. Related works

Image segmentation plays an important role in medical imaging applications. In deep learning domain, segmentation area has been widely utilized to support medical image analysis [20,21]. In [22], the authors developed a multi-label method based on supervised structured for the segmentation of retinal vessels. They applied pre-processing methods before feeding the image into the network. Ortiz et al. [7], in contrast, proposed a deep CNN that ignored pre-processing steps and directly used raw RGB image as input. In [8], the segmentation network was divided into two steps: using multiscale CNN and using fully connected conditional random fields (CRFs).

Thick and thin vessel segmentation were considered using segment-level loss and pixel-wise loss [10]. Similarly, deep vessel segmentation was proposed that achieved high quality vessel probability map using a CNN network and a CRFs layer [12]. The fully CNN network generates probability maps, whereas carry out segmentation using dense global pixel correlation. The authors in [13] utilized stationary wavelet transform with a multiscale fully connected CNN to adapt with the varying width and direction of the vessel structure in the retina. However, aforementioned architectures used multiple steps that increases misclassification error and computational complexity. Several medical image segmentation methods using U-Net-based CNNs have been proposed for solving the segmentation problem and reducing the error rate [16]. The U-Net structure takes care of the sampling that is required to check class-imbalance factors. Furthermore, it is capable of scanning an entire image in just one forward pass, which enables it to consider the full context of the image [23,24]. Hence, this study also considered using U-Net-like CNN architecture to evaluate the efficiency of the proposed regularizers.

Generally, the learning process of the neural network is maximized using task-specific regularization techniques to avoid overfitting and push the sparsity of the network. The authors in [25] proposed a regularizer with scribbles, combining partial cross entropy and normalized cut for weakly-supervised segmentation.

In [17], the authors proposed graph-based smoothing regularizer that treated the network paying attention to small and tiny vessel connections. It treated the image as two graphs by calculating the graph laplacians on the vessel region and background regions. In contrast, in this study we proposed MISO and DISO regularizers based on EC, which calculate the number of isolated objects for accurate segmentation of vessel regions.

3. Proposed methodology

This study proposed EC-based regularizers to estimate the number of isolated objects in U-Net-like deep CNN architecture for delineating small retinal vessel connections on a fundus image. Before training process, we enhanced the dataset with some preprocessing steps. The image is converted into grayscale followed by data normalization and contrast-limited adaptive histogram equalization (CLAHE). We applied normalization to keep the image into the same scale and CLAHE technique to enhance the contrast of the grayscale image.

3.1. Constructing Euler characteristics for the number of isolated objects

Euler characteristic (EC) is a global topology, which invariant to all topological transformations such as rotation and scale. Generally, the EC of a two dimensional image is considered to be the number of connected component minus the number of holes. The objective function of the EC is computed based on the relationship

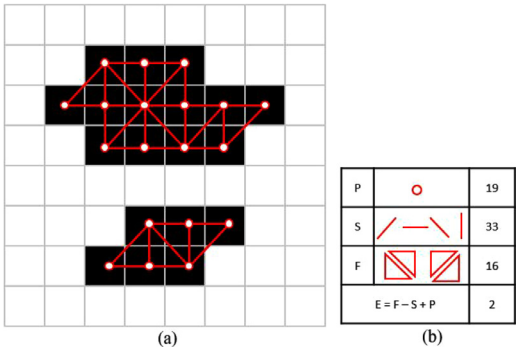

Fig. 2. An example of constructing Euler characteristics using mask patterns (a) illustration showing object (black) pixels based on 8×8 neighborhood pixels. (b) illustration calculating Euler characteristics for the number of isolated object according to the number of vertices (P), sides (S), and faces (F) from object pixels (a).

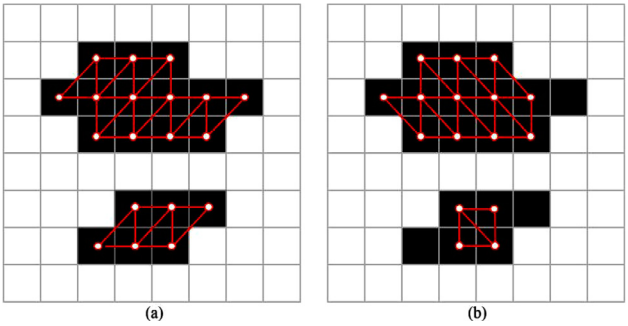

Fig. 3. Two ways of constructing Euler characteristics using mask patterns for triangulation. (a) and (b) show examples of triangulation in opposite direction with each other.

between the number of vertices (P), sides (S), and faces (F) :

$$EC = F - S + P \tag{1}$$

However, in the case of simple polygon without holes, the EC is equal to one. Here we briefly explained how to define the EC effectively by constructing vertices, sides, and faces on 8×8 neighbourhood pixels connectivity using simple mask patterns, as shown in Fig. 2. It calculates EC directly related to the number of isolated objects. The EC on the binary image based on 8×8 neighbourhood pixels can be constructed as follows; 1) transforming object pixel in the image to a vertice, 2) adding a side between the vertices with 8-connectivity without a cross side, 3) summing the number of vertices, 4) summing the number of sides, 5) summing the number of faces or triangles, and finally, 6) calculating EC using Eq. (1). As can be seen in Fig. 2, EC estimated the number of isolated objects as 2, with number of vertices, sides, and faces as 19, 33, and 16 respectively ($EC = F - S + P = 16 - 33 + 19 = 2$).

Furthermore, to address the invariant problem in preserving the vessel connections, we considered constructing vertices, sides, and faces in two different directions. It can be briefly explained using mask patterns on a 8×8 neighbourhood pixels connectivity, as shown in Fig. 3a and b. Then EC is estimated as $EC_1 = F_1 - S_1 + P_1$ and $EC_2 = F_2 - S_2 + P_2$ from Fig. 3a and b, respectively, which is directly related to the number of isolated objects. Finally, the total number of isolated objects E is considered by computing the average between these two directions, which is defined as

$$E = \frac{EC_1 + EC_2}{2} \tag{2}$$

3.2. Network implementation

The regularizer layer based on EC for small vessel connections is evaluated using U-Net-like deep CNN structure. The proposed

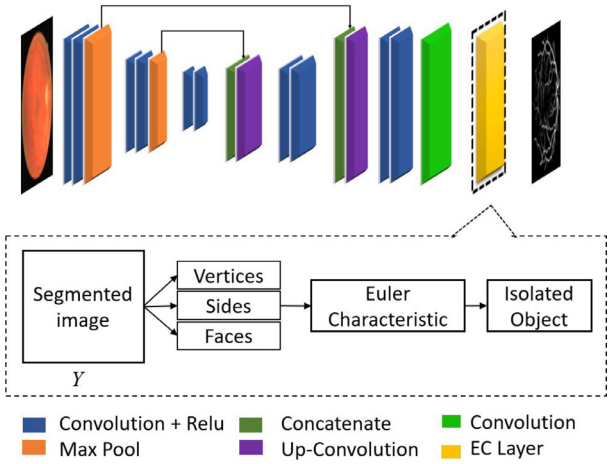

Fig. 4. Proposed architecture using Euler characteristics regularizer.

architecture contains an encoder and decoder module, as shown on Fig. 4. The encoder module includes three blocks. First, two convolutional layers followed by ReLU and max-pooling layer each having 32 feature maps. Second, two convolutional layers followed by ReLU and max-pooling layer with 32 and 64 feature maps, respectively. Third, two convolutional layers each having 128 feature maps. The decoder module contains four convolutional layers followed by ReLU and one convolution layer without ReLU. The output from decoder is upsampled with the factor of 2. After deconvolution the feature maps were concatenated with the encoder layers using skip connections. Then pixel-based probability maps and predictions are generated by a sigmoid classifier function. Finally, after the sigmoid function we employed EC.

By following [26–28], we calculated EC and incorporated this into the network using one layer. Let us consider input image as $X \in \mathbb{R}^{M.N}$, and $T \in \{0,1\}^{M.N}$ be the corresponding groundtruth, with 1 indicating pixels in the vessel and 0 is indicating pixels in the background area. And let us consider f be a U-Net parameterized by weight W. Then the output image of the network is $Y = f(X, W) \in [0,1]^{M.N}$. The binary cross entropy (BCE) loss is used for calculating the vessel region segmentation, which is defied as

$$L_{BCE} = \sum_{i=1} t_i log(y_i) + (1 - t_i) log(1 - y_i) \tag{3}$$

Although U-Net predicts the vessel region, the BCE loss treats every pixel independently. Therefore, it fails to estimate the topological characteristics such as the number of isolated objects on a vessel region. It can be clearly observed as the misclassification of small vessel regions in Fig. 1. This could be accounted to the fact that some pixels exhibit low costs in terms of BCE loss, and thus have large impact on the topology of the predicted results. To address this problem, we proposed a regularizer based on EC that penalized BCE if have many isolated objects comprises the target task.

Therefore, we incorporated EC into the network that retrieved the number of isolated object (E) through the number of vertices, sides, and faces of the segmented regions using the Eqs. (1) and (2). We used E as a regularizer term with the cross entropy cost function to train the proposed network for precisely delineating the small vessel connections. It forced the network to minimize the number of isolated objects by minimizing the misprediction error there are large number of isolated objects, and thus we named it the *MISO* regularizer. It is defined as

$$L_{MISO} = L_{BCE} + \alpha E_{OUT} \tag{4}$$

where α is a scaling parameter to control the regularizer and E_{OUT} represents the number of isolated objects in the segmentation output.

3.3. Regularization based on the differences of number of isolated objects between prediction and groundtruth

In this study, we also investigated the regularizer based on the differences of number of isolated objects between output and groundtruth (DISO) in delineating the vessel regions. Different from MISO, it forces the number of isolated objects between the output and the groundtruth to be equal or more closer. It is defined as

$$L_{DISO} = L_{BCE} + \alpha \left| E_{OUT} - E_{LABEL} \right| \tag{5}$$

where E_{OUT}, E_{LABEL} is number of isolated object of the predicted output and groundtruth, respectively. The DISO based object function leads to large misclassification error if the number of isolated objects between the output and groundtruth is not equal. Otherwise, it produces zero misclassification error in detecting the vessel regions.

3.4. Regularization based on Euler characteristic with graph based smoothing

The regularizer based on GS using a graph laplacian matrix is considered the image into two graph laplacians for vessel regions and background area [17]. In GS, smoothness level on vessel regions (S) and background area is constructed and can be written as

$$S = y^T (L_F + L_B) y = y^T L_G y \tag{6}$$

where L_F and L_B indicates laplacian graph of vessel and background, respectively. In [17], we defined L_{GS} by incorporating GS with binary cross entropy loss, as indicated in the following equation

$$L_{GS} = L_{BCE} + \beta S \tag{7}$$

In this study, we attempted to evaluate the effectiveness of combining our proposed MISO-based EC with GS, thus utilizing the advantages of both the number isolated objects as well as smoothness level of vessel regions. The proposed MISO with GS (GISO) is defined as

$$L_{GISO} = L_{BCE} + \alpha E_{OUT} + \beta S \tag{8}$$

where α and β are scaling parameters to control the regularizer.

4. Experimental setup

4.1. Dataset

The proposed network structure using EC regularizer for accurate vessel segmentation is evaluated on DRIVE, STARE, and CHASEDB1 fundus image datasets. The DRIVE dataset (Canon CR5 nonmydriatic 3CCD camera at 45° field of view) consisted of 40 images with the size 768×584 pixels and 8 bits per color channel taken with the field of view of approximately 540 pixels in diameter [3]. The STARE dataset (TopCon TRV-50 fundus camera at 35° field of view) included 20 images with the size of 605×700 pixel with 24 bits per pixel. The CHASEDB1 dataset included 40 images with the size 999×960 pixels. Considering our aim was evaluating the proposed segmentation error, manual segmentation by an ophthalmologist was used as a reference ground truth image.

4.2. Evaluation and performance measures

The proposed architecture is evaluated on DRIVE, STARE and CHASEDB1 with 20,19 and 20 for training and 20, 1 and 20 for testing, respectively. In order to guarantee that there are enough datasets in training the network, each image is divided into a number of patches with the size 48×48 pixels and thus it successfully increased 4,750 patches on every image. The generalizability of the proposed framework on three different data sets is investigated using the leave-one-out method. The performance of the deep U-Net-like CNN architecture in segmenting blood vessel connections especially the small isolated or thin vessel segmentation is compared with or without our proposed EC-based regularizers. In addition, the performance of the network designed with our proposed L_{MISO} and L_{DISO} in preserving the connectivity of the disconnected vessel pixels is compared with L_{GISO} and our previously proposed GS regularizer in the U-Net-like architecture.

The performance of the network designed with proposed L_{MISO} and L_{DISO} compared with other methods are validated against ground truth through three performance measures : sensitivity (Sn), specificity (Sp) and accuracy (Acc). Sn measures the ability of the proposed structure to detect the vessel pixels. Sp measures the ability of the structure to find non-vessel pixels. Acc calculates the proportion of the predicted vessel pixels that are true vessel pixels. Furthermore, we used receiver operating characteristic curve to compute the area under curve (AUC) value for the measurement of the capability of the proposed system in predicting the vessel pixels.

4.3. Implementation details

We set 100 epochs and batch size to 32. The learning rate is initialized to 0.001 and reduced 10 times at every 25 epoch for ensuring the convergence of the network. We used Adam as the optimization of the network. The regularization parameters α, and β are set to 1e-1 and 1e-5, respectively.

The proposed approach is implemented using Pytorch library with Intel(R) Core(TM) i7-6700K CPU @ 4.00GHz Processor, 32 GB of RAM and Nvidia GeForce GTX 1080/PCIe/SSE2 graphic cards.

5. Results and discussion

The vessel regions with complicated vessel structure shows the intersection of the vessels with large and tiny vessels. It is shown with some representative examples in Fig. 5. It demonstrated that the U-Net-like network without specific regularizer showed poor ability in delineating the vessel with complicated structure. However, if incorporated with our proposed regularizer based on EC, it can accurately identify the detailed vessel junctions and tiny vessels. Table 1 presents the performance comparison of our proposed regularizers in segmenting blood vessel connections, especially small isolated or thin vessel segmentation from background pixels over the architecture without regularizer on different datasets. The proposed network with MISO and DISO regularizer performed well in segmenting the disjoint vessel connections better than the architecture without regularizer. The CNN architecture without our proposed regularizer technique misses a lot of small or thin vessels, which can also be observed in the qualitative results on all dataset. The incapability of the classical BCE-based architecture in detecting thin vessels can also be found out through significantly low Sn values on all three datasets (Table 1). However, the proposed regularization technique efficiently connects the disjoint blood vessels with higher AUC values ($< 95\%$), thus demonstrating the reliability of the proposed network in diagnosing the DR accurately (Fig. 6).

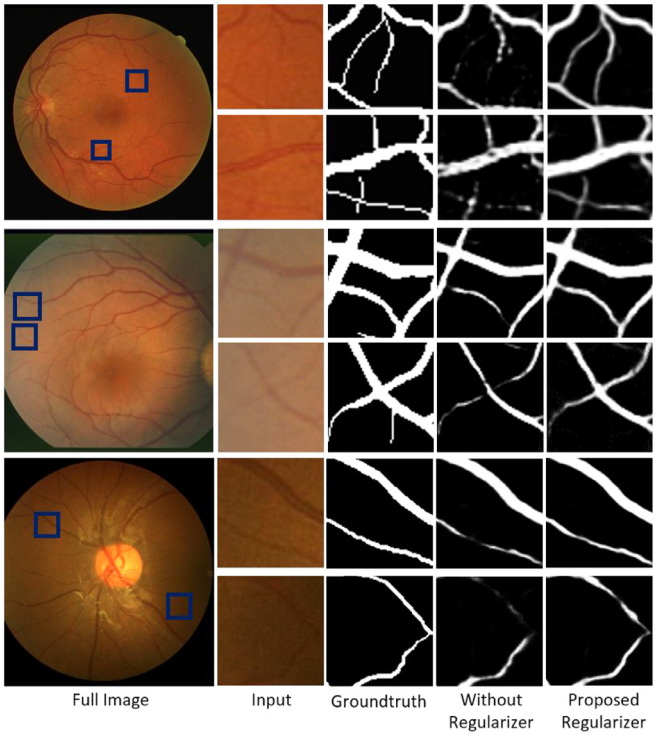

Fig. 5. Segmentation results of the architecture without and with our proposed regularizer for blood vessels on DRIVE (top row), STARE (middle row), and CHASEDB1 (bottom row) datasets.

The performance of the U-Net-like CNN architecture with our proposed EC-based regularizers is compared over the GS and the combined EC with GS regularizers (Table 2). The performance of the combined GISO regularizer revealed almost similar performance with DISO regularizer, demonstrated that the proposed EC-based regularizer efficiently acquired both the smoothness level and isolated pixel level interpretation. Thus, EC-based regularizer shows high potential in learning multiple properties by eliminating two different regularizers in diagnosing the blood vessel connections for DR. The performance of the combined GISO regularizer revealed higher performance than the regularizer using only with GS for vessel detection. It clearly demonstrated that the isolated object regularizer is beneficial in forcing the architecture to learn the segmentation region more effectively.

In addition, to prove the effectiveness of our approach with different α value, we used the MNIH road dataset [29] that has similar vessel-like structure as a fundus image. The performance comparison of our approach with baseline in terms of dice coefficient score (DCS) explains our approach performs better than the baseline with α value at 0.001 (Table 3).

Table 1
Performance comparison of the architecture without and with our proposed Euler characteristic-based regularizer on various datasets.

Regularizer	Sn	Sp	Acc	AUC
DRIVE				
L_{BCE}	0.7583	**0.9826**	0.9551	0.9691
L_{MISO}	0.8463	0.9759	**0.9600**	0.9824
L_{DISO}	**0.8705**	0.9700	0.9578	**0.9825**
STARE				
L_{BCE}	0.6524	**0.9824**	0.9331	0.9370
L_{MISO}	**0.7401**	0.9754	**0.9403**	**0.9546**
L_{DISO}	0.7671	0.9683	0.9382	0.9533
CHASEDB1				
L_{BCE}	0.5812	0.9855	0.9487	0.9567
L_{MISO}	**0.6080**	**0.9879**	**0.9533**	**0.9681**
L_{DISO}	**0.7906**	0.9770	**0.9600**	**0.9786**

Table 2
Performance comparisons of the proposed regularizer over graph-based smoothing and combined graph-based smoothing with isolated object regularizer on various dataset.

Regularizer	Sn	Sp	Acc	AUC
DRIVE				
L_{MISO}	0.8463	0.9759	0.9600	0.9824
L_{DISO}	**0.8705**	0.9700	0.9578	**0.9825**
L_{GS}	0.7802	**0.9854**	**0.9602**	0.9817
L_{GISO}	0.8621	0.9721	0.9586	**0.9825**
STARE				
L_{MISO}	0.7401	0.9754	**0.9403**	0.9546
L_{DISO}	0.7671	0.9683	0.9382	0.9533
L_{GS}	**0.7739**	0.9650	0.9365	0.9499
L_{GISO}	0.7096	**0.9806**	0.9402	**0.9548**
CHASEDB1				
L_{MISO}	0.6080	**0.9879**	0.9533	0.9681
L_{DISO}	**0.7906**	0.9770	**0.9600**	**0.9786**
L_{GS}	0.7427	0.9799	0.9583	0.9752
L_{GISO}	0.7364	0.9817	0.9594	0.9757

5.1. Performance comparison against state-of-the-arts

The proposed EC-based regularizer network is compared of state-of-the-art methods (Table 4). Our proposed approach achieved 0.9824 of AUC and 0.9600 of accuracy, which is higher than the other existing methods. This can be attributed to the fact that this study considered the branches of blood vessels as almost connected with each other, which means the vessel structure has only one isolated object in which all thin vessels are connected or exhibits minimum number of isolated objects. Hence, our proposed regularizer produced acceptable results by pushing the network to make the output region consisting minimum number of isolated objects.

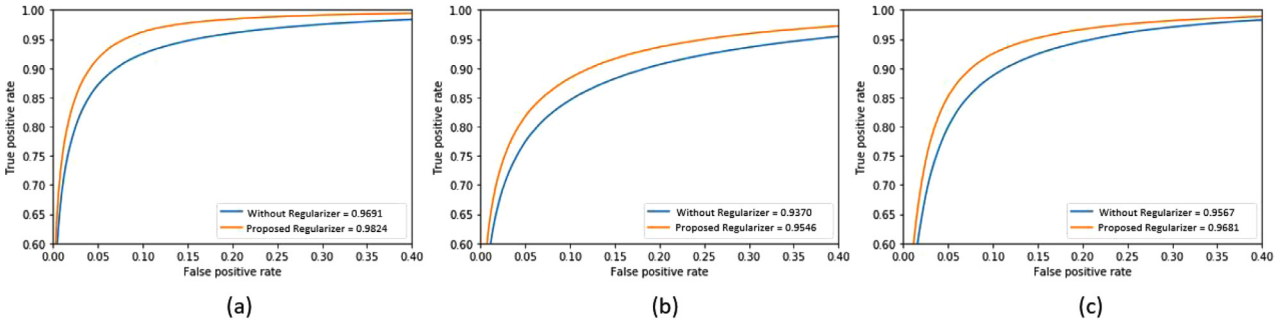

Fig. 6. Performance comparisons of the architecture without and with our proposed regularizer using receiver operating characteristics curve analysis on different datasets. (a) DRIVE (b) STARE and (c) CHASEDB1.

Table 3
Performance comparison of our proposed method with baseline on the MNIH road dataset.

Regularizer	**Parameter** α	DCS
L_{DICE} (Baseline)	-	0.8782
$L_{DICE} + \alpha E_{OUT}$	0.01	0.8748
$L_{DICE} + \alpha E_{OUT}$	0.001	**0.8856**
$L_{DICE} + \alpha E_{OUT}$	0.0001	0.8775

Table 4
Performance comparison of the proposed approach with state-of-the-art methods.

Methods	Sn	Sp	Acc	AUC
Azzopardi [30]	0.7655	0.9704	0.9442	0.9614
Li et al. [31]	0.7569	0.9816	0.9527	0.9738
Liskowski [32]	0.7763	0.9768	0.9495	0.972
Fu et al. [12]	0.7603	-	0.9523	-
Dasgupta et al. [22]	0.7691	0.9801	0.9533	0.9744
Roychowdhury [33]	0.725	**0.983**	0.952	0.962
Chen et al. [34]	0.7426	0.9735	0.9453	0.9516
Yan et al. [10]	0.7653	0.9818	0.9542	0.9752
Yan et al. [35]	0.7631	0.982	0.9538	0.975
Jin et al. [14]	0.7963	0.98	0.9566	0.9802
Proposed method	**0.8463**	0.9759	**0.9600**	**0.9824**

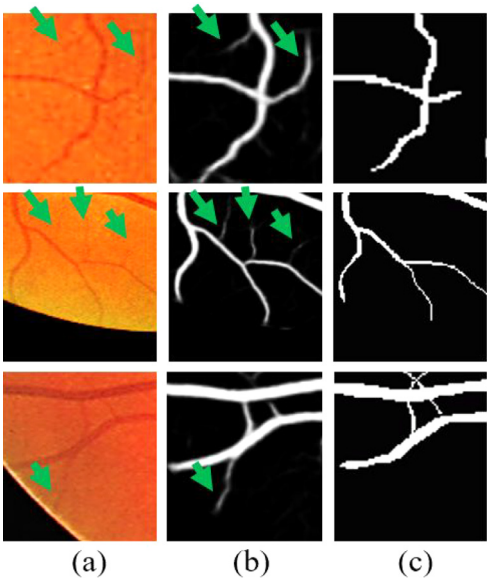

Fig. 7. Performance comparison of the proposed method with ground truth in predicting small vessels along with the large vessels. (a) input images, (b) prediction results (green arrow indicates small vessel detection) (c) ground truths (missing annotation of small vessels compared to the input image). (For interpretation of the references to color in this figure legend, the reader is referred to the web version of this article)

Though the qualitative performance of our method is much better than the other methods, the quantitative computation based on the given ground truth shows almost similar accuracy and AUC value compared with the state-of-the-art methods. This is because of the missing annotation of the small vessels in the ground truth misleading the measurements and considering the predicted small vessels as false positives (Fig. 7). Moreover, experts ignored the small vessels due to the low contrast conditions or noise artifacts; our approach proved its efficiency in detecting small vessels even in the low quality images as well.

The other reasons of the proposed network showed lesser Sp than the other methods may be the regions such as fovea, optical disk, and lesion detected in unhealthy fundus image distracted

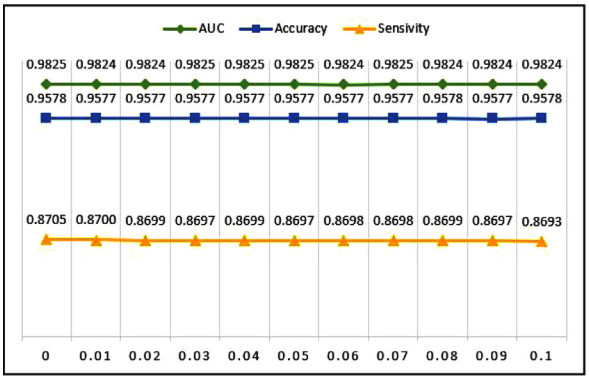

Fig. 8. Noise sensitivity evaluation on DRIVE dataset interms of AUC, accuracy and sensitivity. Evaluating Gaussian noise with the ranges of 0.01 to 0.1.

the network training. However, including the other class information in the training may suppress the misclassification and could improve the Sp value. Compared with the existing architectures, our proposed architecture is simple and accurate. In [14], the U-Net architecture included deformable convolutional block layer in encoder and decoder part increased the computational complexity with large number of dimensions. Whereas, in our approach, we simply added one layer to evaluate the EC to calculate the number of isolated objects from the output of the last layer for accurate detection of vessel regions. Though our approach proved its capability in delineating the small branches and disconnected vessel regions better than the conventional architectures, the EC is estimated by treating pixel-by-pixel cost computational time. Thus, there is room for further improvement of the proposed regularizer to make it less computational costs.

5.2. Sensitivity to noise evaluation for segmentation

We conducted experiments to evaluate the sensitivity of the segmentation achieved by our method to noise. We used the test set of the DRIVE dataset and added Gaussian noise with different levels of noise variances (from 0.01 to 0.1). As shown in Fig. 8, our approach delineated the vessels with the AUC values ranging from 0.9824 to 0.9825, accuracy values ranging from 0.9577 to 0.9578 and sensitivity values ranging from 0.8693 to 0.8705. The small increasing variations of detection performance value (0.0001) with increasing levels of noise is observed, which demonstrates that the proposed approach is robust to noise.

5.3. Measure of complexity of learning

We investigated the measures of complexity of learning of our approach over the other methods during inference stage. We chose the computational complexity of deep learning and non deep learning methods (Table 5). We compared the computational complexity of learning between deep learning and non-deep learning methods and found that our approach does not show much differences compared with other methods. Furthermore, the measures of complexity of learning time of the baseline network is almost similar with ours. It indicates the addition of regularization term with the existing architecture does not tend to increase the execution time and hence the complexity of learning of our approach is not sensitive to the performance of detection.

Though our approach is effective and accurate to identify the connectivity of pixels, it poses the restriction on implementing on the tree-like objects. The boundary cannot be well defined if the algorithm encounters any loop-like objects, which is the limitation of this study. However, it can be addresed using a suitable regularizer based on an high-quality ground truth. In future work, we

Table 5
Performance comparison of the measure of complexity of learning of the proposed approach with the state-of-the-art methods.

Method	Time	Architecture
Azzopardi et al. [30]	10s	Non-Deep learning
Staal et al. [3]	15m	Non-Deep learning
Roychowdhury [33]	2.5s	Non-Deep learning
Liskowskiet al. [32]	92s	CNN
Luo et al. [36]	31.17s	SIFCN
Fu et al. [12]	1.3s	DeepVessel
Tan et al. [37]	10m	CNN
Jin et al. [14]	15.3s	DUNet
U-Net (Baseline)	23s	U-Net
Proposed Method	23s	U-Net+EC Regularizer

plan to extend the proposed regularizer using the graph theory approach to estimate the number of isolated objects on image. Furthermore, it would be efficient to incorporate the vessel regions and lesions segmentation in one end-to-end network. This study also suggested that the proposed segmentation approach may be useful in non-medical applications that contains vessel-like structures, such as palmprints segmentation for biometric systems.

6. Conclusion

This study proposed EC-based regularizers to estimate the number of isolated objects in U-Net-like deep CNN architecture for delineating small retinal vessel connections on a fundus image. The proposed EC-based MISO and DISO regularizers approach demonstrated improvement in retaining the width of the small and disjointed vessel connectivities through its high AUC values. Our approach can segment more number of vessels and can reconnect all isolated vessels, which is superior than the performance of the baseline architecture not using the proposed regularizer. Furthermore, it also demonstrated that the isolated objects regularizer is beneficial in forcing the architecture to learn the smoothness and isolated pixel level of interpretation of vessel regions. Compared with other state-of-the-art methods, the EC-based regularizer improved the performance in localizing and connectivity between the pixels of the vessel regions with high acceptable value of AUC value. These findings indicate that the proposed system could be a highly reliable detection system for DR.

Declaration of Competing Interest

The authors declare that they have no known competing financial interests or personal relationships that could have appeared to influence the work reported in this paper.

Acknowledgments

This work was partly supported by JSPS KAKENHI grant number 16K00239 and 18F18112.

References

[1] B.E. Kobrin Klein, Overview of epidemiologic studies of diabetic retinopathy, Ophthalmic Epidemiol. 14 (4) (2007) 179–183.
[2] C. Wilson, M. Horton, J. Cavallerano, L.M. Aiello, Addition of primary care-based retinal imaging technology to an existing eye care professional referral program increased the rate of surveillance and treatment of diabetic retinopathy, Diabetes Care 28 (2) (2005) 318–322.
[3] J. Staal, M.D. Abramoff, M. Niemeijer, M.A. Viergever, B. Van Ginneken, Ridge-based vessel segmentation in color images of the retina, IEEE Trans. Med. Imaging 23 (4) (2004) 501–509, doi:10.1109/TMI.2004.825627.
[4] D. Primitivo, R. Alma, C. Erik, V. Arturo, C. Edgar, P.-C. Marco, Z. Daniel, A hybrid method for blood vessel segmentation in images, Biocybern. Biomed. Eng. 39 (3) (2019) 814–824.
[5] M.M. Fraz, P. Remagnino, A. Hoppe, B. Uyyanonvara, A.R. Rudnicka, C.G. Owen, S.A. Barman, Blood vessel segmentation methodologies in retinal images–a survey, Comput. Methods Programs Biomed. 108 (1) (2012) 407–433.
[6] C. Kirbas, F. Quek, A review of vessel extraction techniques and algorithms, ACM Comput. Surv. (CSUR) 36 (2) (2004) 81–121.
[7] B. Ortiz, J. Ram, F.J. Mart, Retinal blood vessel segmentation by multi-channel deep convolutional autoencoder, in: International Joint Conference SOCO'18-CISIS'18-ICEUTE'18, vol. 771, 2019, pp. 37–46, doi:10.1007/978-3-319-94120-2.
[8] K. Hu, Z. Zhang, X. Niu, Y. Zhang, C. Cao, F. Xiao, X. Gao, Retinal vessel segmentation of color fundus images using multiscale convolutional neural network with an improved cross-entropy loss function, Neurocomputing 309 (2018) 179–191, doi:10.1016/j.neucom.2018.05.011.
[9] L. Luo, D. Chen, D. Xue, Retinal blood vessels semantic segmentation method based on modified U-Net, in: Proceedings of the 30th Chinese Control and Decision Conference, CCDC 2018, IEEE, 2018, pp. 1892–1895, doi:10.1109/CCDC.2018.8407435.
[10] Z. Yan, X. Yang, K.-T. Cheng, Joint segment-level and pixel-wise losses for deep learning based retinal vessel segmentation, IEEE Trans. Biomed. Eng. 65 (9) (2018) 1912–1923.
[11] K.-K. Maninis, J. Pont-Tuset, P. Arbelaez, L. Van Gool, Deep retinal image understanding, in: International Conference on Medical Image Computing and Computer-Assisted Intervention, Springer, 2016, pp. 140–148.
[12] H. Fu, Y. Xu, S. Lin, D.W.K. Wong, J. Liu, DeepVessel: retinal vessel segmentation via deep learning and conditional random field, in: International Conference on Medical Image Computing and Computer-Assisted Intervention, Springer, 2016, pp. 132–139.
[13] A. Oliveira, S. Pereira, C.A. Silva, Retinal vessel segmentation based on fully convolutional neural networks, Expert Syst. Appl. 112 (2018) 229–242.
[14] Q. Jin, Z. Meng, T.D. Pham, Q. Chen, L. Wei, R. Su, DUNet: a deformable network for retinal vessel segmentation, Knowl.-Based Syst. 178 (2019) 149–162.
[15] S. Lian, L. Li, G. Lian, X. Xiao, Z. Luo, S. Li, A global and local enhanced residual U-Net for accurate retinal vessel segmentation, IEEE Comput. Archit. Lett. (2019). 1–1
[16] O. Ronneberger, P. Fischer, T. Brox, U-Net: convolutional networks for biomedical image segmentation, in: International Conference on Medical Image Computing and Computer-Assisted Intervention, Springer, 2015, pp. 234–241.
[17] L. Hakim, N. Yudistira, M.S. Kavitha, T. Kurita, U-Net with graph based smoothing regularizer for small vessel segmentation on fundus image, in: International Conference on Neural Information Processing, Springer, 2019, pp. 515–522.
[18] M.H. Chen, P.F. Yan, A fast algorithm to calculate the Euler number for binary images, Pattern Recognit. Lett. 8 (5) (1988) 295–297, doi:10.1016/0167-8655(88)90078-5.
[19] J.L. Diaz De Leon Santiago, J.H. Sossa-Azuela, On the computation of the Euler number of a binary object, Pattern Recognit. 29 (3) (1996) 471–476, doi:10.1016/0031-3203(95)00098-4.
[20] M.S. Kavitha, T. Kurita, S.Y. Park, S.I. Chien, J.S. Bae, B.C. Ahn, Deep vector-based convolutional neural network approach for automatic recognition of colonies of induced pluripotent stem cells, PLoS ONE 12 (12) (2017) 1–18, doi:10.1371/journal.pone.0189974.
[21] M. Kavitha, C.-H. Lee, K. Shibudas, T. Kurita, B.-C. Ahn, Deep learning enables automated localization of the metastatic lymph node for thyroid cancer on 131 I post-ablation whole-body planar scans, Sci. Rep. 10 (1) (2020) 1–12.
[22] A. Dasgupta, S. Singh, A fully convolutional neural network based structured prediction approach towards the retinal vessel segmentation, in: Proceedings - International Symposium on Biomedical Imaging, 2017, pp. 248–251, doi:10.1109/ISBI.2017.7950512.
[23] N. Yudistira, M.S. Kavitha, T. Itabashi, A.H. Iwane, T. Kurita, Prediction of sequential organelles localization under imbalance using a balanced deep U-Net, Sci. Rep. 10 (1) (2020) 1–11, doi:10.1038/s41598-020-59285-9.
[24] M. Kavitha, N. Yudistira, T. Kurita, Multi instance learning via deep CNN for multi-class recognition of Alzheimer's disease, in: 2019 IEEE 11th International Workshop on Computational Intelligence and Applications (IWCIA), IEEE, 2019, pp. 89–94.
[25] M. Tang, A. Djelouah, F. Perazzi, Y. Boykov, C. Schroers, Normalized cut loss for weakly-supervised CNN segmentation, in: Proceedings of the IEEE Computer Society Conference on Computer Vision and Pattern Recognition, vol. 1, 2018, pp. 1818–1827.
[26] N. Otsu, T. Kurita, A new scheme for practical flexible and intelligent vision systems., in: MVA, 1988, pp. 431–435.
[27] T. Kurita, A. Hidaka, Statistical pattern recognition and discriminant analysis, first ed., Corona Publishing CO., LTD, Tokyo, JPN, 2019.
[28] T. Kobayashi, Trainable co-occurrence activation unit for improving convnet, in: 2018 IEEE International Conference on Acoustics, Speech and Signal Processing (ICASSP), IEEE, 2018, pp. 1273–1277.
[29] V. Mnih, Machine Learning for Aerial Image Labeling, University of Toronto (Canada), 2013.
[30] G. Azzopardi, N. Strisciuglio, M. Vento, N. Petkov, Trainable COSFIRE filters for vessel delineation with application to retinal images, Med. Image Anal. 19 (1) (2015) 46–57.
[31] Q. Li, B. Feng, L. Xie, P. Liang, H. Zhang, T. Wang, A cross-modality learning approach for vessel segmentation in retinal images, IEEE Trans. Med. Imaging 35 (1) (2016) 109–118, doi:10.1109/TMI.2015.2457891.
[32] P. Liskowski, K. Krawiec, Segmenting retinal blood vessels with deep neural networks., IEEE Trans. Med. Imaging 35 (11) (2016) 2369–2380.

[33] S. Roychowdhury, D.D. Koozekanani, K.K. Parhi, Blood vessel segmentation of fundus images by major vessel extraction and subimage classification, IEEE J. Biomed. Health Inf. 19 (3) (2014) 1118–1128.
[34] Y. Chen, A labeling-free approach to supervising deep neural networks for retinal blood vessel segmentation, arXiv preprint arXiv:1704.07502(2017).
[35] Z. Yan, X. Yang, K.-T. Cheng, A three-stage deep learning model for accurate retinal vessel segmentation, IEEE J. Biomed. Health Inf. 23(4) (2018) 1427–1436.
[36] Y. Luo, H. Cheng, L. Yang, Size-invariant fully convolutional neural network for vessel segmentation of digital retinal images, in: 2016 Asia-Pacific Signal and Information Processing Association Annual Summit and Conference (APSIPA), IEEE, 2016, pp. 1–7.
[37] J.H. Tan, U.R. Acharya, S.V. Bhandary, K.C. Chua, S. Sivaprasad, Segmentation of optic disc, fovea and retinal vasculature using a single convolutional neural network, J. Comput. Sci. 20 (2017) 70–79.